A theta-like sum from diffraction physics

1999 J. Phys. A: Math. Gen. 32 L329

(http://iopscience.iop.org/0305-4470/32/28/101)

J. Phys. A: Math. Gen. **32** (1999) L329–L336. Printed in the UK PII: S0305-4470(99)03969-4

LETTER TO THE EDITOR

A theta-like sum from diffraction physics

M V Berry
H H Wills Physics Laboratory, Tyndall Avenue, Bristol BS8 1TL, UK

Received 5 May 1999, in final form 24 May 1999

Abstract. For large n, graphs of the modulus of the sum $S_n(x) = (2n)!2^{-2n}\sum_{m=-n}^{n}\exp(\mathrm{i}\pi x m^2)\{(n-m)!(n+m)!\}^{-1}$ exhibit self-similar structure. $S_n(x)$ can be closely approximated by a theta function near its natural boundary. An exact renormalization enables this function to be calculated efficiently, and an approximate arithmetic renormalization explains the self-similarity. Atomic diffraction experiments could enable the self-similarity to be detected in the laboratory.

Exact solution of Schrödinger's equation (Berry 1998) shows that the sum

$$S_n(x) = \frac{(2n)!}{2^{2n}}\sum_{m=-n}^{n}\frac{\exp(\mathrm{i}\pi x m^2)}{(n-m)!(n+m)!} \tag{1}$$

gives the amplitude of the nth-order beam of atoms diffracted by a 'crystal of light' (volume grating) (Oberthaler *et al* 1996) of thickness x, interacting with the atoms via a complex (that is, non-Hermitian) potential (proportional to $\exp(\mathrm{i}Ky)$) (Keller *et al* 1997), when the beam is incident normally on the crystal. $S_n(x)$ has the special values

$$S_n(0) = 1 \qquad S_n(1) = 0 \tag{2}$$

and the symmetries

$$S_n(x+2) = S_n^*(-x) = S_n(x) \tag{3}$$

so that it suffices to study only the range $0 \leqslant x \leqslant 1$. Of special interest is the behaviour of $S_n(x)$ as $n \to \infty$. Computations (figure 1) suggest that in this asymptotic limit self-similarity emerges, and my purpose here is to explain it.

The terms in (1) decay rapidly as $|m|$ increases, because, from Stirling's formula,

$$\frac{1}{(n-m)!(n+m)!} \approx \frac{\exp(2n)}{2\pi n^{2n+1}}\exp(-m^2/n) \qquad (n \to \infty, |m| \ll n). \tag{4}$$

This shows that the significant terms are those with $|m| < \sqrt{n}$, so that $S_n(x)$ has structure down to scales $\Delta x \sim 1/n$. Thus

$$S_n(x) \approx f(x, 1/\pi n) \tag{5}$$

where $f(x, y)$ is a Jacobi theta function (Abramowitz and Stegun 1972) which it is convenient to write as

$$\begin{aligned} f(x, y) &= \sqrt{y}\sum_{m=-\infty}^{\infty}\exp(\mathrm{i}\pi x m^2)\exp(-\pi y m^2) \\ &= \sqrt{y}\theta_3(0, \exp\{\mathrm{i}\pi(x + \mathrm{i}y)\}). \end{aligned} \tag{6}$$

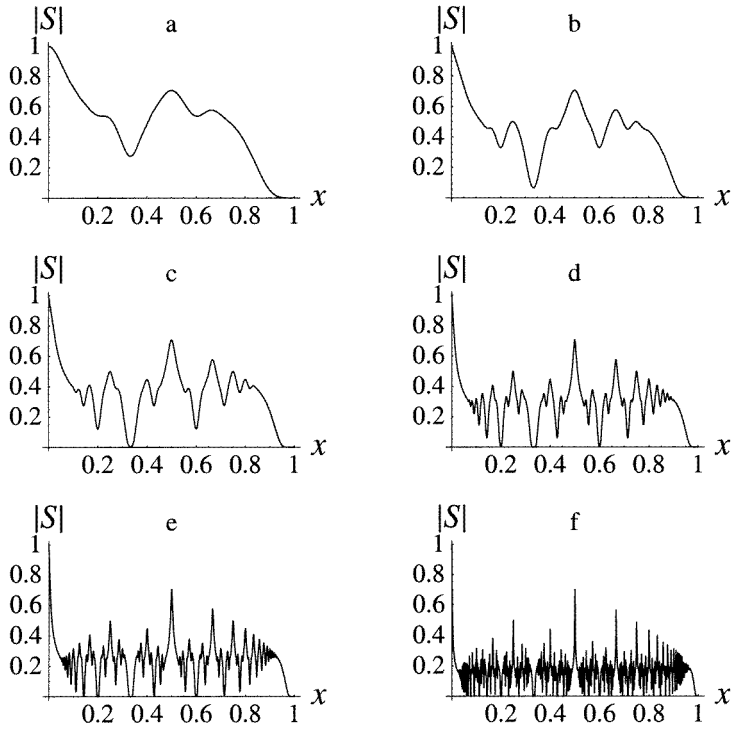

Figure 1. Emergent self-similarity in the graph of $|S_n(x)|$ versus x as n increases. (*a*) $n = 5$, (*b*) $n = 10$, (*c*) $n = 20$, (*d*) $n = 50$, (*e*) $n = 100$, (*f*) $n = 500$.

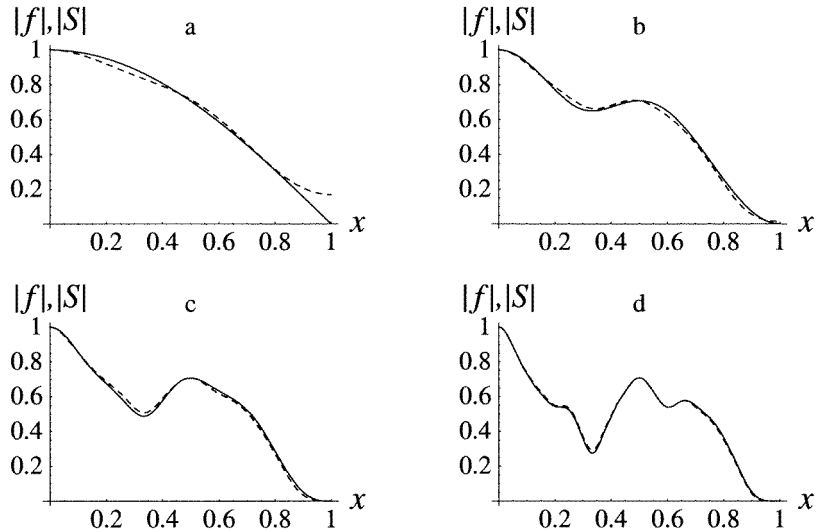

Figure 2. Comparison of $|S_n(x)|$ (full curves) with $|f(x, 1/\pi n)|$ (equation (5)) (dashed curves). (*a*) $n = 1$, (*b*) $n = 2$, (*c*) $n = 3$, (*d*) $n = 5$.

As figure 2 shows, (5) is an excellent approximation, even when n is not large.

Therefore we seek to understand $f(x, y)$ for small y (large n), that is, near the natural

boundary of the theta function, where the convergence of the sum in (6) is poor. Clearly, $f(x, y)$ has structure down to a scale $\Delta x \sim y$. To explore this structure, we employ several tools from the extensive literature on theta functions (see, in particular, Marklof 1990a, b and references therein). Many of these tools are well known; our aim here is the modest one of using them to explain the self-similarity observed in computations.

Note first the symmetries (cf (3))

$$f(x+2, y) = f^*(-x, y) = f(x, y) \tag{7}$$

that allow x to be reduced to the interval $0 \leqslant x \leqslant 1$, and the reflection identity (based on $(-1)^{m^2} = (-1)^m$)

$$\begin{aligned} f(1-x, y) &= \sqrt{y} \sum_{m=-\infty}^{\infty} \exp(-\mathrm{i}\pi x m^2) \exp(-\pi y m^2)(-1)^m \\ &= f^*(4x, 4y) - f^*(x, y) \end{aligned} \tag{8}$$

that enables f for x near 1 to be evaluated in terms of f for x near 0.

The theta-function identity (a special case of the Poisson sum formula, Lighthill (1958) transforms (6) into

$$f(x, y) = \sqrt{y + \mathrm{i}x}\, f^*\left(\frac{x}{x^2+y^2}, \frac{y}{x^2+y^2}\right). \tag{9}$$

Using the symmetries (7), and defining

$$k(x, y) \equiv \left[\frac{x}{x^2+y^2}\right] \tag{10}$$

(where here and hereafter $[u]$ will denote the integer part of u), and the map

$$\begin{aligned} \mathbf{M}: x \to u(x, y) &= \begin{cases} \dfrac{x}{x^2+y^2} \pmod 1 & (k(x, y) \text{ even}) \\ 1 - \dfrac{x}{x^2+y^2} \pmod 1 & (k(x, y) \text{ odd}) \end{cases} \\ y \to v(x, y) &= \frac{y}{x^2+y^2} \end{aligned} \tag{11}$$

we obtain the fundamental *renormalization transformation*

$$f(x, y) = \sqrt{y + \mathrm{i}x}\, \mathbf{K}^{1+k(x,y)} f(u(x, y), v(x, y)) \tag{12}$$

where $\mathbf{K}$ denotes the operation of complex conjugation.

Applied to $x = 0$, (12) gives

$$f(0, y) = \sqrt{y} f(0, 1/y) = \sum_{m=-\infty}^{\infty} \exp(-\pi m^2/y) \to 1 \qquad \text{as} \quad y \to 0 \tag{13}$$

and for $x = 1$, with (8),

$$\begin{aligned} f(1) &= \sqrt{4y} f(0, 1/(4y)) - \sqrt{y} f(0, 1/y) \\ &= \sum_{m=-\infty}^{\infty} \{\exp(-\pi m^2/(4y)) - \exp(-\pi m^2/y)\} \to 0 \qquad \text{as} \quad y \to 0. \end{aligned} \tag{14}$$

Convergence of (6) can be improved by repeatedly applying the renormalization (12), since when $r \equiv \sqrt{(x^2+y^2)} < 1$ the value of y increases under the map $\mathbf{M}$. $\mathbf{M}$ divides the strip $0 \leqslant x \leqslant 1$, $0 \leqslant y \leqslant \infty$ into zones defined by the value of $k(x, y)$ (figure 3): the zone k lies between neighbouring semicircles with radii $1/(2k)$, centred on $x = 1/(2k)$. Because y increases under $\mathbf{M}$, any initial point (x, y) must eventually reach the zone $k = 0$. The

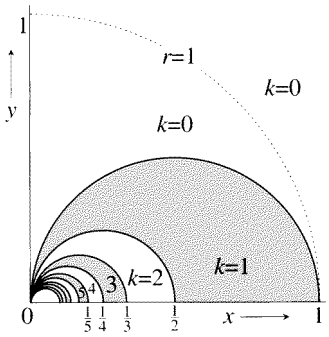

Figure 3. Zones corresponding to different values of k in the map **M** defined by (11).

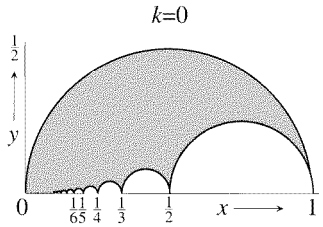

Figure 4. The shaded points are those satisfying (15), that map into the $k = 0$ zone under one application of **M**.

quarter-circle $r = 1$ divides this zone into pairs of points (x, y) and $(x, y)/r^2$ that are stable period-2 orbits to which any initial point not in the zone $k = 0$ is attracted by **M**. For points in the $k = 0$ zone, convergence is slowest on the circle $r = 1$, where the terms of the series (6) are $\exp\{-\pi m^2\sqrt{(1-x^2)}\}$; this is poor near $x = 1$, but then the reflection law can be used, giving a series with terms $\exp\{-\pi m^2\sqrt{((1+x)/(1-x))/8}\}$, that converges faster than without reflection if $x > \frac{7}{8}$ (even when $x = \frac{7}{8}$—the worst convergence of all—the terms are $\exp\{-\pi m^2(\sqrt{15})/8) = \exp\{-1.52m^2\}$).

Most points not in the $k = 0$ zone land there after one application of **M**. These are the points (figure 4) satisfying

$$\left(x - \frac{1}{2}\right)^2 + y^2 < \frac{1}{4} \qquad \left(x - \frac{k+\frac{1}{2}}{k(k+1)}\right)^2 + y^2 > \left(\frac{1}{2k(k+1)}\right)^2 \qquad (k = 1, 2, \ldots). \tag{15}$$

They constitute a fraction $4 - \pi^2/3 = 0.7103$ of the area in the zones $k \geqslant 1$. The remaining points map into the $k = 0$ zone after more than one application of **M**. Points close to the x-axis require many applications, and it is these, with $y \ll 1$, that hide the self-similarity we seek to understand.

When $y \ll 1$, we can define

$$q(x) = \left[\frac{1}{x}\right] \tag{16}$$

and **M** defined by (11) can be approximated by

$$\begin{aligned} \mathbf{N}: x \to \xi(x) &= \begin{cases} \dfrac{1}{x} \pmod 1 & (q(x) \text{ even}) \\ 1 - \dfrac{1}{x} \pmod 1 & (q(x) \text{ odd}) \end{cases} \\ y \to \eta(x, y) &= \frac{y}{x^2}. \end{aligned} \tag{17}$$

This generates the *approximate renormalization*

$$f(x, y) \approx \exp(\tfrac{1}{4}\mathrm{i}\pi)\sqrt{x}\mathbf{K}^{1+q(x)} f(\xi(x), \eta(x, y)). \tag{18}$$

For the modulus $|f(x, y)|$ this becomes

$$|f(x, y)| \approx \sqrt{x}|f(\xi(x), \eta(x, y))|. \tag{19}$$

N is closely related to the Gauss map for continued fractions; its ergodic properties have been studied in detail (Berry and Goldberg 1988, Marklof 1999a) in connection with the renormalization analysis not only of theta functions but also of the finite sums $g(L, x) = \sum_{m=1}^{L} \exp(\mathrm{i}\pi x m^2)$ (there, the emphasis was on the curves—'curlicues'—drawn in the complex g plane as L increases for fixed x; the curves depend sensitively on the arithmetic nature of x).

To expose the self-similarity, we study the interval

$$\frac{1}{2m+1} \leqslant x \leqslant \frac{1}{2m-1} \tag{20}$$

by writing

$$x = \frac{1}{2m-u} \qquad (-1 \leqslant u \leqslant +1). \tag{21}$$

For $u > 0$, $q(x) = 2m-1$ is odd; for $u \leqslant 0$, $q(x) = 2m$ is even. Application of (19) leads to

$$\left| f\left(\frac{1}{2m-u}, y\right)\right| \approx \frac{1}{\sqrt{2m-u}} |f(u, (2m-u)^2 y)|. \tag{22}$$

This shows that the graph of $|f(x, y)|$ in the unit x interval is contained in either half of the interval (20), which is $4m^2-1$ times smaller, with the graph in the smaller interval calculated for a y value that is $4m^2$ times smaller.

An immediate application of this renormalization, together with (13) and (14), gives

$$\left| f\left(\frac{1}{2m}, y\right)\right| \approx \frac{1}{\sqrt{2m}} \qquad f\left(\frac{1}{2m+1}, y\right) \approx 0. \tag{23}$$

As figure 5 shows, this reproduces $|f|$ accurately over a range of m values that gets larger as y gets smaller.

Iteration of the approximate renormalization $n+1$ times enables the graph to be reduced to the smaller intervals

$$x_0(u) = \cfrac{1}{2m_0 + \cfrac{\varepsilon_1}{2m_1 + \cfrac{\varepsilon_2}{2m_2 + \cdots \cfrac{\varepsilon_n}{2m_n - u}}}} \qquad (-1 \leqslant u \leqslant +1, \varepsilon_m = \pm 1). \tag{24}$$

Defining the successively mapped x values as

$$x_s = \cfrac{1}{2m_s + \cfrac{\varepsilon_{s+1}}{2m_{s+1} + \cdots \cfrac{\varepsilon_n}{2m_n - u}}} \tag{25}$$

the renormalization gives

$$|f(x_0(u), y)| \approx \sqrt{\prod_{s=0}^{n} x_s(u)}\left| f\left(u, y \Big/ \prod_{s=0}^{n} x_s(u)^2\right)\right|. \tag{26}$$

The approximation is valid while the y value on the right-hand side is much smaller than unity. This corresponds to renormalizing down to, but not beyond, an n value corresponding to the fine scale $\Delta x \sim y$. For larger n, the exact renormalization (11) and (12) must be used, attracting to the period-2 orbit in the $k = 0$ zone.

Figure 6 demonstrates the efficiency of the approximate renormalization for three nested magnifications of the original graph, corresponding to $m_0 = 3$, $m_1 = 2$, $m_2 = 2$, $\varepsilon_1 = -1$,

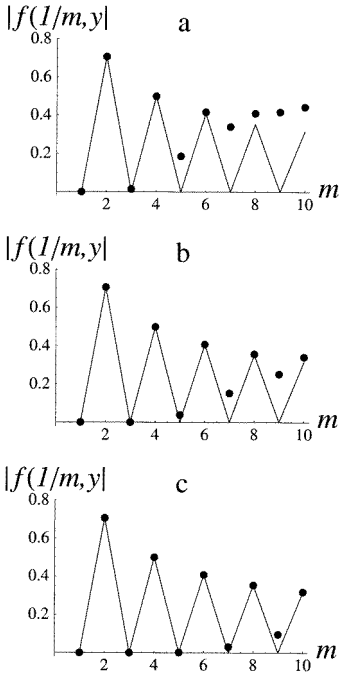

Figure 5. Test of approximate renormalization for (*a*) $y = 0.02$, (*b*) $y = 0.01$, (*c*) $y = 0.005$. Dots: exact values of $|f|$; full lines: rhs of (23). The renormalization should fail when the width of the x-interval (2) equals the fine scale $\Delta x \sim y$ of the graph, that is when $m \sim 1/\sqrt{(2y)}$, giving $m = 5$, 7.1 and 10 for (*a*), (*b*) and (*c*), respectively.

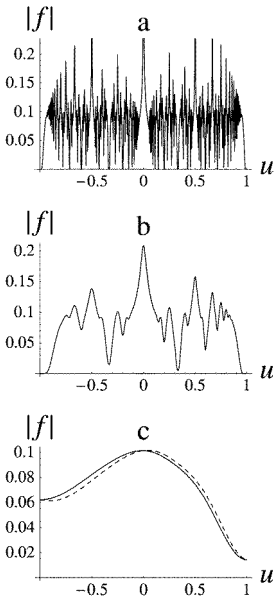

Figure 6. Self-similarity, illustrated by comparing magnifications of graphs of the exact $|f(x, y)|$ (full curves) with the predictions of the approximate renormalization (27) (dashed curves), for $y = 0.000\,05$. The magnified intervals are (*a*) $\frac{1}{7} = 0.142\,857 \leqslant x \leqslant \frac{1}{5} = 0.2$, (*b*) $\frac{5}{29} = 0.172\,414 \leqslant x \leqslant \frac{3}{17} = 0.174\,442$, (*c*) $\frac{13}{75} = 0.173\,333 \leqslant x \leqslant \frac{21}{121} = 0.173\,444$. (In (*a*) and (*b*) the exact and approximate curves are indistinguishable.)

$\varepsilon_2 = +1$, giving the predictions

$$\left| f\left(\frac{1}{6-u}, y\right)\right| \approx \frac{1}{\sqrt{6-u}}|f(u, (6-u)^2 y)| \tag{27a}$$

$$\left| f\left(\frac{1}{6-u-\dfrac{1}{4-u}}, y\right)\right| \approx \frac{1}{\sqrt{23-6u}}|f(u, (23-6u)^2 y)| \tag{27b}$$

$$\left| f\left(\frac{1}{6-u-\dfrac{1}{4-u+\dfrac{1}{4-u}}}, y\right)\right| \approx \frac{1}{\sqrt{98-23u}}|f(u, (98-23u)^2 y)|. \tag{27c}$$

In spite of the self-similarity, the graph of $|f(x, y)|$ in the limit $y \to 0$ is not fractal in the sense of being a continuous nondifferentiable curve with dimension $1 < D \leqslant 2$. This can be seen from the following explicit formula for values of f when $y = 0$, that follows from the renormalization (or averaging the familiar Gauss sums) and is a special case of corollary 3.3

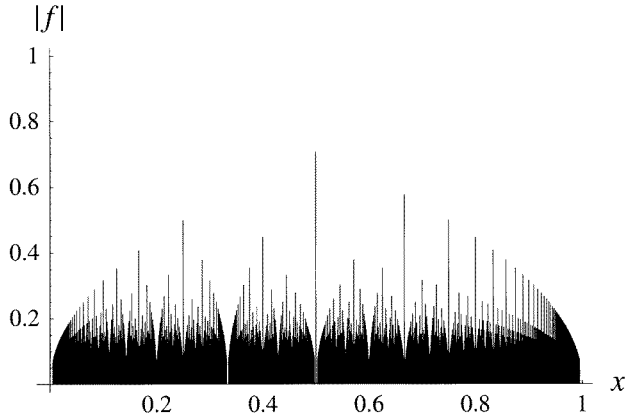

Figure 7. Graph of $|f(x,0)|$ from equation (28) including all p/q with $q \leqslant 200$.

in Marklof (1999b):

$$\begin{aligned} |f(p/q,0)| &= \frac{1}{\sqrt{q}} \qquad x = p/q \qquad (p \text{ or } q \text{ even}) \\ &= 0 \qquad x = p/q \qquad (p, q \text{ both odd}) \\ &= 0 \qquad x \text{ irrational.} \end{aligned} \tag{28}$$

This is shown in figure 7; all previous graphs of $|f|$ and $|S|$ can be understood as smoothings of this picture.

Another way to guess that the limiting curve is not continuous as $y \to 0$ is to note from (6) that the coefficient of the oscillating exponential $\exp(\mathrm{i}\pi x m^2)$ is roughly constant for $|m| < 1/\sqrt{y}$, beyond which it decays rapidly. Therefore the limiting power spectrum is that of a series with constant coefficients and frequencies $\omega \sim n^2$, namely $\mathrm{d}n/\mathrm{d}\omega \sim \omega^{-\beta}$, where $\beta = \frac{1}{2}$, from which the rule $D = (5-\beta)/2$ (Orey 1970, Berry and Lewis 1980) gives, formally, $D = \frac{9}{4}$, indicating that the limiting graph is not only nondifferentiable but noncontinuous.

Finally, we note that the complex potential giving rise to the diffraction amplitudes (1) has been realized in the laboratory (Keller *et al* 1997), raising the possibility that the self-similar structures explored here could be seen experimentally.

I thank J Marklof for kindly reminding me of the result (28), and D Zagier for helpful remarks.

References

Abramowitz M and Stegun I A 1972 *Handbook of Mathematical Functions* (Washington: National Bureau of Standards)

Berry M V 1998 Lop-sided diffraction by absorbing crystals *J. Phys. A: Math. Gen.* **31** 3493–502

Berry M V and Goldberg J 1988 Renormalization of curlicues *Nonlinearity* **1** 1–26

Berry M V and Lewis Z V 1980 On the Weierstrass-Mandelbrot fractal function *Proc. R. Soc.* A **370** 459–84

Keller K, Oberthaler M K, Abfalterer R, Bernet S, Schmiedmayer J and Zeilinger A 1997 Tailored complex potentials and Friedel's law in atom optics *Phys. Rev. Lett.* **79** 3327–30

Lighthill M J 1958 *Introduction to Fourier Analysis and Generalized Functions* (Cambridge: Cambridge University Press)

Marklof J 1999a Limit theorems for theta sums *Duke. Math. J.* **97** 127–53

Marklof J 1999b Theta sums, Eisenstein series, and the semiclassical dynamics of a precessing spin *Emerging Applications of Number Yheory* ed D Hejhal (New York: Springer) pp 405–50

Oberthaler M K, Abfalterer R, Bernet S, Schmiedmayer J and Zeilinger A 1996 Atom waves in crystals of light *Phys. Rev. Lett.* **77** 4980–3

Orey S 1970 Gaussian sample functions and the Hausdorff dimension of level crossings *Z. Wahrscheinlichkeitstheorie* **15** 249–56